

Advanced Beam Shaping for Ultrafast Laser Micro-processing



O. J. Allegre, J. Ouyang, W. Perrie, Y. Jin, S. P. Edwardson, and G. Dearden

Abstract This paper details the use of novel beam shaping methods to improve the flexibility and speed of ultrafast laser micro-processes. The vector fields of a picosecond-pulse laser beam are shaped using a Spatial Light Modulator (SLM) and polarization optics, so that both the amplitude and direction of the electric field vectors are controlled with a high spatial resolution. This allows to shape the focal field landscapes obtained by focusing the beam with a low Numerical Aperture (NA) lens. A number of shaped vector beams are produced, including radially or azimuthally polarized vortex beams. All these beams are then used for surface ablation of titanium alloy substrates at low fluence to imprint Laser Induced Periodic Surface Structures (LIPSS). Thanks to their polarization dependent properties, LIPSS help to analyse the vector fields in the focal region. This analysis reveals for the first time how the orbital angular momentum associated with a vortex vector field induces complex focal field landscapes which fluctuate along the optical axis of the focusing lens. The produced shaped focal fields are also used for helical micro-drilling stainless steel and silicon substrates. The results are compared in terms of quality and efficiency, illustrating how the distinct machining properties associated with each beam make it best suited for specific processes or materials.

Keywords Beam shaping · Vector beam · Polarization · Ultrafast

O. J. Allegre (✉)

Department of Mechanical, Aerospace and Civil Engineering, The University of Manchester, Manchester M13 9PL, UK

e-mail: olivier.allegre@manchester.ac.uk

J. Ouyang · W. Perrie · Y. Jin · S. P. Edwardson · G. Dearden

Laser Group, School of Engineering, University of Liverpool, Liverpool L69 3GQ, UK

© Springer Nature Switzerland AG 2022

S. Hinduja et al. (eds.), *Proceedings of the 38th International MATADOR Conference*, https://doi.org/10.1007/978-3-319-64943-6_8

1 Introduction

The last few years have seen increased research activity in the field of laser microprocessing with ultrashort pulses (pulse-length <10 ps), where the laser energy interacts with the workpiece material with very little thermal damage and allows sub-micron resolution features to be manufactured [1]. A number of processes have benefited from this, including the drilling of fuel-injection nozzles [1], the dicing of silicon wafers, or the nanotexturing of biomedical functional surfaces [2]. Despite their potential, the low speed and lack of flexibility of early ultrashort-pulse laser microprocessing systems slowed down their industrial uptake. New methods to improve efficiency without decreasing quality would further expand the range of applications that benefit from these processes.

Laser beams with a space-variant electric field orientation and/or amplitude are often referred to as vector beams [3]. They include the beams with a radial or azimuthal polarization as well as those which carry an orbital angular momentum (i.e. beams with an optical vortex field). Recent studies have explored the use of vector beams in short-pulse laser microprocesses such as surface structuring, drilling and cutting [3, 4]. These early results highlighted the great potential of vector beams for improving ultrafast laser process efficiency and speed without compromising quality.

However, these early results were limited in scope and mainly compared beams with a pure radial and azimuthal polarization (i.e. without orbital angular momentum). Higher order vector beams with more complex fields which may be beneficial for specific ultrafast processes have not yet been investigated. Thus, in this paper we use an industrial picosecond-pulse laser processing system with a Spatial Light Modulator (SLM) and polarization optics to produce a number of vector beams, including radially and azimuthally polarized beams with and without an orbital angular momentum. The low Numerical Aperture (NA) focusing properties of each vector beam is analysed in detail. These beams are then used for helical drilling stainless steel and silicon substrates and the results are compared in terms of quality and efficiency.

2 Experimental Details

The experimental setup is shown in Fig. 1. The laser source is a High-Q picosecond-pulse laser system (10 ps pulse width, 1064 nm wavelength, $M^2 < 1.3$, 2W maximum average power, 50 kHz maximum repetition rate and a horizontal linear polarization output). The beam vector fields are structured using a SLM (Hamamatsu X10468-03) and a waveplate (S-waveplate, Altechna or quarter-waveplate, Newport), to convert the incident linearly polarized beam into a cylindrical vector beam or a circularly polarized beam respectively. A 4-f system (Lens 1 and 2 in Fig. 1) re-images the produced beam vector fields into the 10 mm input aperture of a scanning galvo (Nutfield). At the galvo output, the beam is focused with a flat field f-theta lens ($f =$

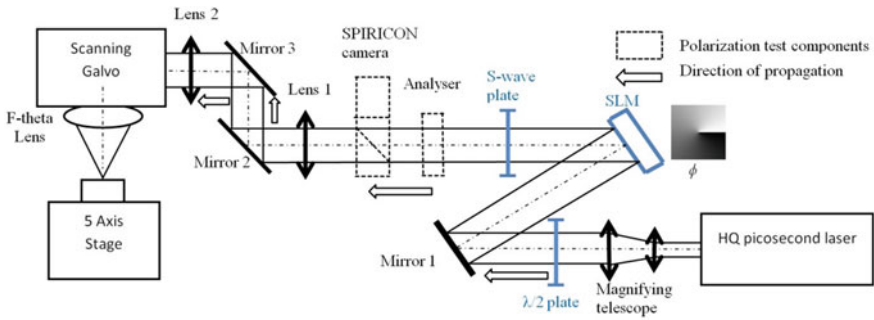


Fig. 1 Experimental setup used to shape the vector field of a picoseconds-pulse laser microprocessing system

100 mm). For the surface ablation and drilling experiments, samples are mounted on a precision 5-axis motion control system (Aerotech) allowing accurate positioning in the focal plane. Prior to processing the samples, the beam is analyzed with a rotating polarizing filter and a SPIRICON beam profiler (see Fig. 1).

In the experiments, a number of beam vector field configurations are produced by tilting the S-waveplate optical axis to various angles. Henceforth, vector beams with a radial, an azimuthal, or an intermediate tilted polarization (see Fig. 2) are referred to as RP, AP and IP beams respectively. A circularly polarized beam is also used in some of the experiments, produced by replacing the S-waveplate with its fast axis tilted to 45°. This is referred to as CP beam

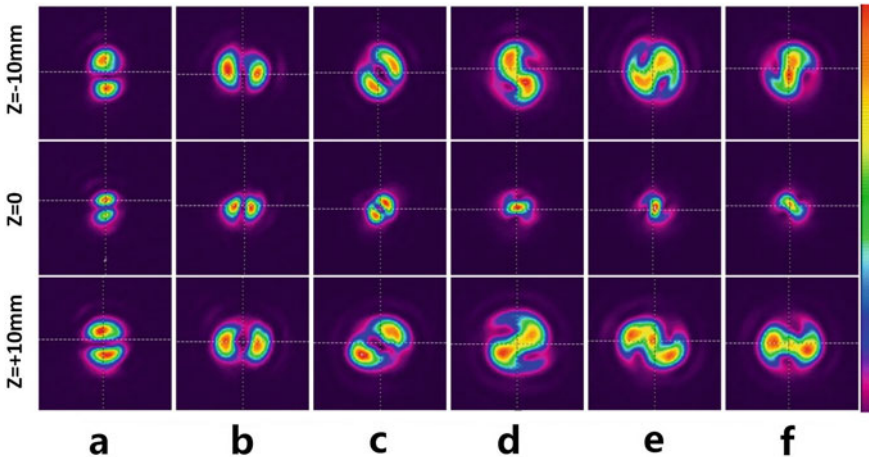


Fig. 2 Intensity profiles of the focused beam, observed at various Z coordinates along the optical axis ($Z = 0$ at focal plane, middle row). **a** RP beam. **b** AP beam. **c** IP beam. **d** RPOAM beam. **e** APOAM beam. **f** IPOAM beam. Intensity in arbitrary unit, transmission axis of polarizing filter oriented vertically

henceforth. For comparison purposes, an orbital angular momentum is then added to all these beams by using the SLM to induce an optical vortex phase wavefront with a topological charge value of $l = 1$, with the waveplate configured as before. Henceforth, the radially, azimuthally, intermediately and circularly polarized beams with an orbital angular momentum are referred to as RPOAM, APOAM, IPOAM and CPOAM respectively.

3 Results and Discussion

3.1 Analysis of Focal Fields

A first method for analysing the focal fields consists in projecting the focused beam through the polarizing filter onto the SPIRICON profiler, located in a range of places along the optical axis of a focusing lens (Lens 1 in Fig. 1). The resulting intensity profiles shown in Fig. 2 reveal a clear distinction between the vector beams with and without orbital angular momentum. The RP, AP and IP beams with no angular momentum have a distinct double-lobe intensity profile (Fig. 2a–c), typical of annular vector beams [4], which is invariant as it propagates along the optical axis of the focusing lens (apart from the obvious scale factor, proportional to the distance away from the focal plane, see Fig. 2). On the other hand, all the beams with orbital angular momentum have a profile with non-zero intensity at the centre (Fig. 2d–f). It can be seen that the intensity profile varies significantly along the optical axis. At the focal plane, the profile is mostly Gaussian with peak intensity in the centre and has an approximate elliptical shape (see middle row in Fig. 2d–f). Note the long axis of the ellipse is dependent on the incident polarization (i.e. horizontal or vertical when the incident beam is radially or azimuthally polarized respectively, see Fig. 2d, e respectively).

3.2 Surface Processing

To better understand the focal field properties, a second focal analysis method is used: each vector beam in turn is used to produce laser ablation spots (and thus imprint its intensity distribution) on the surface of titanium alloy samples (Ti6Al4V) placed in the focal region of the f-theta lens (Fig. 1). Using a laser fluence near the ablation threshold of the titanium alloy results in the growth of microscopic Laser Induced Periodic Surface Structures (LIPSS) within the ablation spots. The wavelength-sized LIPSS typically develop orthogonally to the local electric field vectors [5] and thus enable to analyse the vector field landscapes in the focal region [6], with a better accuracy than the optical analysis method above. The surface of the titanium samples is placed in a range of positions above or below the focal plane, producing patterns

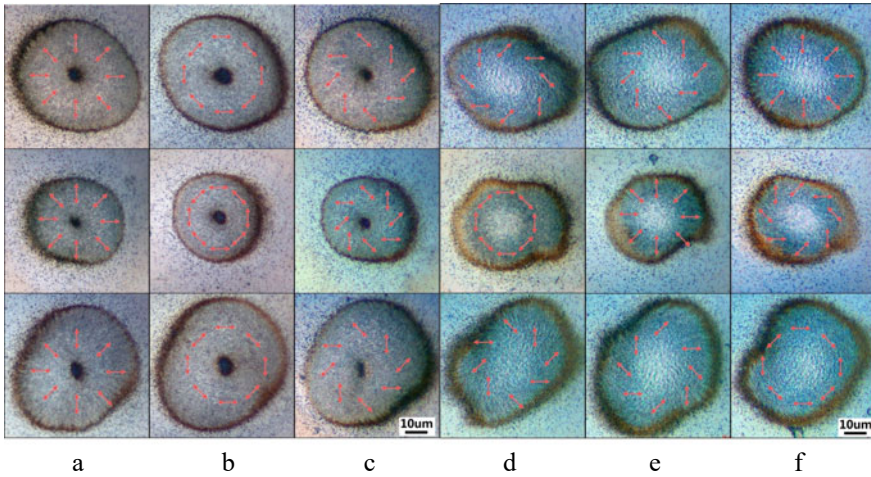


Fig. 3 Optical micrographs showing the laser ablation spots produced along the optical axis with **a** RP beam, **b** AP beam, **c** IP beam, **d** RPOAM beam, **e** APOAM beam, **f** IPOAM beam. The ablation spots have been produced 500 μm above the focal plane (top row), at the focal plane (middle row), and 500 μm below the focal plane (bottom row). The red arrows indicate the polarization direction in each location

of LIPSS at each location. These locations are referred to as observation planes henceforth. For all the surface ablation experiments, the laser output is attenuated to produce an average fluence of $\sim 0.4 \text{ J/cm}^2$ on the sample surface. The samples are exposed for a duration of 10 ms (~ 50 pulses at 5 kHz pulse repetition rate) whilst the beam remains static with regards to the sample. After laser exposure, the produced ablation spots are imaged with an optical microscope (see optical micrographs in Fig. 3).

The ablation spots produced when the incident beam is RP, AP or IP with no orbital angular momentum have a clear annular structure with zero intensity in its central region (Fig. 3a–c), which is consistent with that expected when focusing cylindrical vector beams with a low NA lens [4]. LIPSS are produced with a high uniformity within the ablation spots and indicate that the polarization state is maintained in all observation planes, with no variation along the optical axis of the focusing lens. Note the IP beam with an intermediate tilted polarization (Fig. 2c) produces LIPSS patterns with a spiral shape (see Fig. 3c).

The ablation spots produced when the incident beams had an orbital angular momentum of $l = 1$ are shown in Fig. 3d–e. The geometry of the laser spots, with deeper ablation in the centre than around the edges, was consistent with a Gaussian-like intensity profile (albeit with some distortions due to steps in the vortex phase-maps induced with the SLM). From Fig. 3, it can be seen that LIPSS have been produced around the edges, but not in the centre of the focal spots. Further ablation experiments with various fluence values showed that it was extremely difficult to produce clear LIPSS in the centre of the laser focal spots. Furthermore, the incident

RPOAM beam produced a focal spot with LIPSS oriented in a radial pattern. As LIPSS are orthogonal to the local electric field [5], this suggests that the focal field was azimuthally polarized in these regions. These results show that incident radially and azimuthally polarized beams with an orbital angular momentum of $l = 1$ typically produce a partial inversion of the polarization state at the focal plane. Looking at the fields away from the focal plane in Fig. 3, we can see that the patterns of LIPSS (and corresponding vector field landscape) clearly fluctuate along the optical axis of the focusing lens, in such a way that the states of polarization in the observation planes 500 μm above and below the focal plane are orthogonal to each other (see top and bottom rows in Fig. 3d–f). For example the incident IPOAM beam produces a mostly radial polarization state at the observation plane 500 μm above the focal plane (top micrograph in Fig. 3f). As the beam propagates to the observation plane 500 μm below the focal plane, the polarization changes to a mostly azimuthal state (bottom micrograph in Fig. 3f). These important experimental results demonstrate the variability of the focal fields along the optical axis due to the orbital angular momentum and have significant implications for micromachining.

3.3 Microdrilling

Having demonstrated the ability to shape the focal fields into various complex landscapes, we now investigate the micromachining properties of some of these vector beams (i.e. RP, AP, RPOAM and APOAM beams). For comparison purposes, we also use linearly and circularly polarized Gaussian and annular beams (the latter are simply obtained by inducing an orbital angular momentum of $l = 1$ to the linearly or circularly polarized Gaussian beams). We carry out helical drilling of stainless steel 302 sheets (370 and 500 μm thick) and silicon wafers (500 μm thick) which are typical processes used in industrial micromachining. All the drilling tests use a pulse energy of 80 μJ (i.e. an average fluence of 11.3 J/cm^2 at the focal plane) with a pulse repetition rate of 10 kHz, and the beam is scanned continuously along a circular path with a 100 μm diameter and a 20 mm/s scan speed, using various laser exposure durations. These tests are repeated a number of times with each vector beam to average the results. After laser drilling, all the results are analysed with an optical microscope.

First, the results are assessed qualitatively by comparing the relative size, shape and edge quality of the drilled holes. Figures 4, 5 and 6, which show typical holes drilled in the silicon and steel substrates, highlight significant differences in the hole geometry produced with AP and APOAM beams (i.e. with an annular and Gaussian focal intensity profile respectively). This is especially visible with the exit holes, which are larger and smoother in the latter case (see for example Fig. 6a and b). In fact, the APOAM beam produces holes which are more similar to those made with the CP Gaussian beam (see exit holes, Fig. 6c). It is noted that the linearly polarised (LP) beam produces the worst drilling quality, (see for example Fig. 4d).

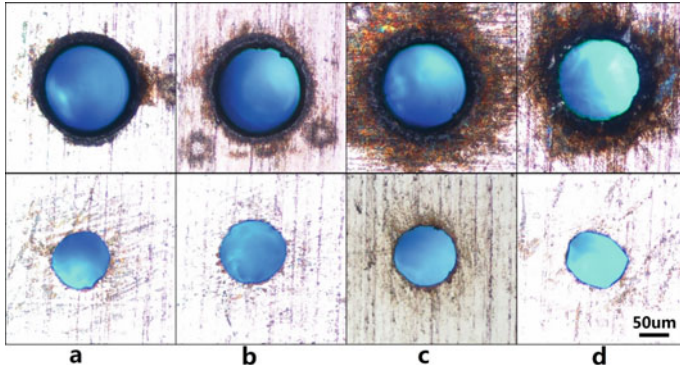


Fig. 4 Optical micrographs showing drilling results on 370 μm stainless steel sheet with: **a** AP, **b** APOAM, **c** CP and **d** LP beams at ~ 20 s laser exposure duration. Top row showing the entrance and bottom row the exit

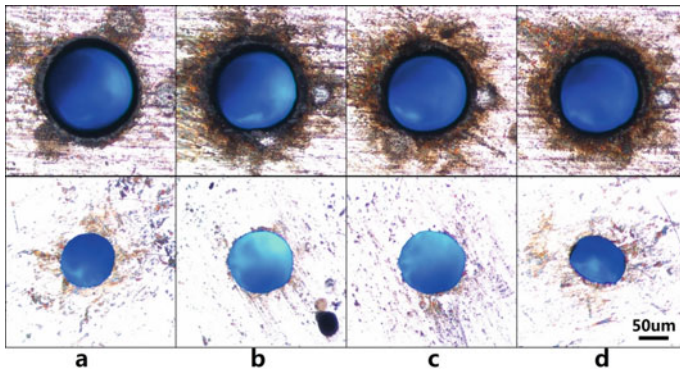


Fig. 5 Optical micrographs showing drilling results on 500 μm stainless steel sheet with: **a** AP, **b** APOAM, **c** CP and **d** LP beams at ~ 70 s laser exposure duration. Top row showing the entrance and bottom row the exit

Next, we evaluate the drilling efficiency of the vector beams by measuring the diameter of the produced holes entrance and exit. The average diameter of holes drilled in the silicon and stainless steel plates are plotted in Fig. 7. Looking at the results obtained in the 500 μm thick silicon and 500 μm thick steel plates, the most noticeable feature is the similarity in the drilling characteristics of the RPOAM, APOAM and CP beams, since they all produce comparable hole geometries ($\sim 125 \mu\text{m}$ diameter entrance and $\sim 112 \mu\text{m}$ diameter exit for example in silicon i.e. a sidewall half-angle taper of $\sim 1.5^\circ$). On the other hand, the RP and AP beams *without* angular momentum have broadly similar characteristics as the CPOAM beam (producing holes of $\sim 142 \mu\text{m}$ diameter entrance and $\sim 84 \mu\text{m}$ diameter exit in silicon i.e. a significantly larger half-angle taper of $\sim 6.6^\circ$). These results can be understood since the former set of beams all produces Gaussian like focal intensity profiles,

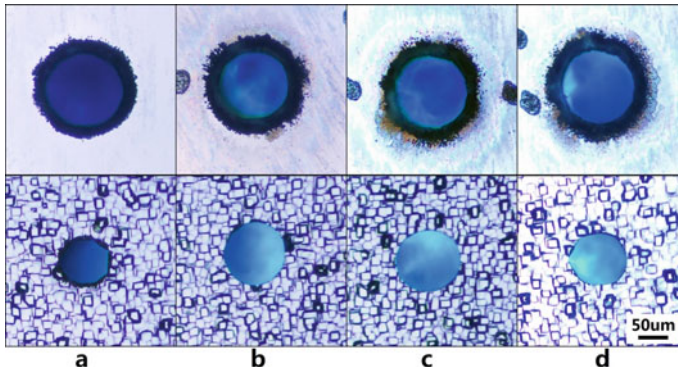


Fig. 6 Optical micrographs showing drilling results on 500 μm silicon wafer with: **a** AP, **b** APOAM, **c** CP and **d** LP beams at ~ 140 s laser exposure duration. Top row showing the entrance and bottom row the exit

whereas the latter produces annular profiles with a lower peak intensity. In other words, the drilling properties in the 500 μm thick silicon and steel plates are more influenced by the focal intensity distribution than the state of polarization

Looking at the drilling results in the 370 μm thick stainless steel plate (Fig. 7), it can be seen that the distinction between the drilling properties of the annular beams (i.e. RP, AP and CPOAM) and those of the Gaussian beams (i.e. RPOAM, APOAM and CP) is less obvious than with the thicker plates. Within the set of annular beams, there is a clear influence of polarization on the diameter of the exit holes. The RP beam produces.

A $\sim 10\%$ larger exit diameter than the AP beam (~ 94 μm vs. ~ 86 μm). This is the result of the better coupling efficiency of radial polarization, which mostly produces *p*-polarized internal reflections on the sidewalls during drilling [3, 4]. On the other hand, azimuthal polarization mostly produces *s*-polarized internal reflections, with a higher reflectivity that leads to increased losses through the hole exit aperture and thus a poorer coupling efficiency overall. The CPOAM beam produces an intermediate exit hole diameter (~ 87 μm). This results from the average of *p*- and *s*-polarized internal reflections during drilling typically seen with circular polarization [6], thus an intermediate coupling efficiency between that of radial and azimuthal polarization. Note that the RPOAM and APOAM beams induce a hybrid state of polarization at the focal plane as demonstrated in Sect. 3.2, and thus both produce exit holes with fairly similar diameters. In summary, these results illustrate how the beam vector fields can be tailored to specific applications requirements. By shaping the focal intensity profile and polarization distribution, the machining properties can be optimized for a given process or material. For example for an application requiring holes with reduced taper in 500 μm thick silicon wafers (i.e. entrance and exit holes of similar diameter), a drilling process with a RPOAM or APOAM would be most appropriate, since it produces the lowest taper angle.

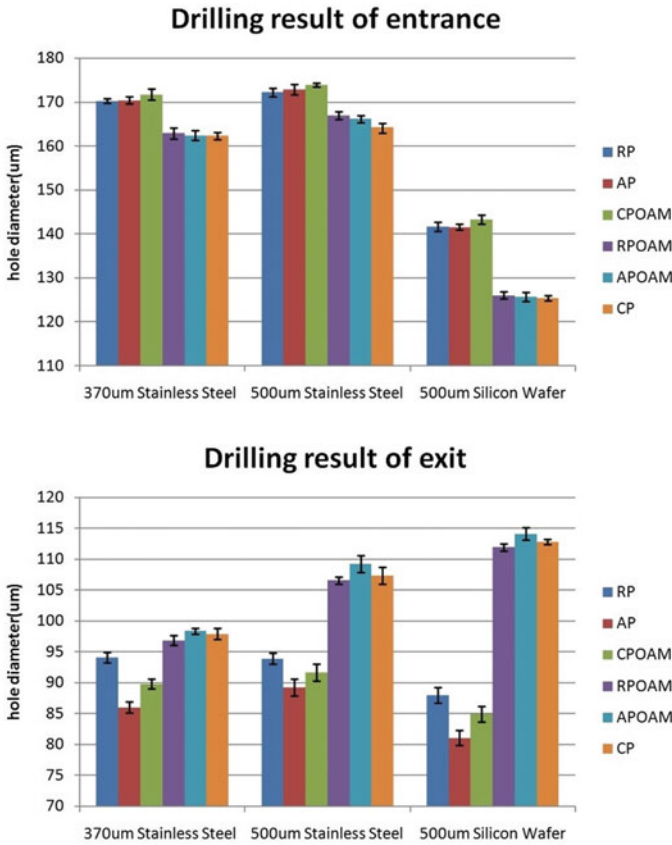


Fig. 7 Average diameter of drilled hole entrance (top) and exit (bottom) in 370 μm thick stainless steel sheets (~ 20 s laser exposure duration), 500 μm thick stainless steel sheets (~ 70 s exposure duration), 500 μm thick silicon wafer (~ 140 s exposure duration) using shaped focal fields

4 Conclusions

In this paper, we have used novel beam shaping methods to accurately control the focal fields of ultrashort-pulse laser beams and influence their micromachining properties. A linearly polarized picosecond-pulse laser beam was structured using an SLM and waveplates, so as to produce radially and azimuthally polarized beams with or without orbital angular momentum. The vector fields obtained by focusing these beams with a low NA lens were analyzed by imprinting LIPSS on polished titanium alloy samples at near-threshold fluences. This revealed for the first time how the orbital angular momentum associated with a vortex wavefront induces structured field landscapes which fluctuate along the optical axis of the focusing lens. The produced vector beams were used for helical drilling, showing how the intensity profile and state of polarization in the focal plane influence the processing speed and

quality. These results illustrate how tailored vector beams can be used to optimize laser microprocesses. The great advantage of the method described here is its flexibility, with an almost infinite range of optical field combinations. Future work will further explore this potential, optimizing vector beams configurations for specific laser micromachining processes.

References

1. Breiting D, Ruf A, Dausinger F (2004) Fundamental aspects in machining of metals with short and ultrashort laser pulses. *Proc SPIE* 5339:49–63
2. Stratakis E, Ranella A, Fotakis C (2011) Biomimetic micro/nanostructured functional surfaces for microfluidic and tissue engineering applications. *Biomicrofluidics* 5(1):013411
3. Allegre OJ, Perrie W, Edwardson SP, Dearden G, Watkins KG (2012) Laser microprocessing of steel with radially and azimuthally polarized femtosecond vortex pulses. *J Opt* 14(8):85601
4. Weber R, Michalowski A, Abdou-Ahmed M, Onuseit V, Kraus M, Graf T (2011) Effects of radial and tangential polarization in laser material processing. *Phys Procedia* 12:21–30
5. Guosheng Z, Fauchet PM, Siegman AE (1982) Growth of spontaneous periodic surface structures on solids during laser illumination. *Phys Rev B* 26(10):5366–5381
6. Allegre OJ, Perrie W, Bauchert K, Dearden G, Watkins KG (2012) Real-time control of polarisation in ultra-short-pulse laser micro-machining. *Appl Phys A* 107(2):445–454